ORIGINAL ARTICLE

The Voyage of Metals in the Universe from Cosmological to Planetary Scales: the need for a Very High-Resolution, High Throughput Soft X-ray Spectrometer

F. Nicastro[1] ⬤ · J. Kaastra[2] · C. Argiroffi[3] · E. Behar[4] · S. Bianchi[5] · F. Bocchino[6] ·
S. Borgani[7] · G. Branduardi-Raymont[8] · J. Bregman[9] · E. Churazov[10,11] ·
M. Diaz-Trigo[12] · C. Done[13] · J. Drake[14] · T. Fang[15] · N. Grosso[16] ·
A. Luminari[17,1] · M. Mehdipour[2] · F. Paerels[18] · E. Piconcelli[1] · C. Pinto[19] ·
D. Porquet[16] · J. Reeves[20] · J. Schaye[21] · S. Sciortino[6] · R. Smith[14] · D. Spiga[22] ·
R. Tomaru[23] · F. Tombesi[17] · N. Wijers[21] · L. Zappacosta[1]

Abstract

Metals form an essential part of the Universe at all scales. Without metals we would not exist, and the Universe would look completely different. Metals are primarily produced via nuclear processes in stars, and spread out through winds or explosions, which pollute the surrounding space. The wanderings of metals in-and-out of astronomical objects are crucial in determining their own evolution and thus that of the Universe as a whole. Detecting metals and assessing their relative and absolute abundances and energetics can thus be used to trace the evolution of these cosmic components. The scope of this paper is to highlight the most important open astrophysical problems that will be central in the next decades and for which a deep understanding of *the Universe's wandering metals, their physical and kinematical states, and their chemical composition* represents the only viable solution. The majority of these studies can only be efficiently performed through High Resolution Spectroscopy in the soft X-ray band.

✉ F. Nicastro
fabrizio.nicastro@inaf.it

Extended author information available on the last page of the article.

1 Introduction

Metals[1] form an essential part of the Universe at all scales. Without metals we would not exist, and the cosmos would look completely different. Metals are primarily born through nuclear processes in stars. They leave their cradles through winds or explosions, and then start their journey through space. This can lead them in and out of astronomical objects on all scales, ranging from comets, planets, stars, entire galaxies, groups and clusters of galaxies to the largest structures of the Universe. Their wanderings are often fundamental in determining how these objects, and the entire Universe, evolve and reach their current states and configurations.

Because the majority of the ordinary matter in the Universe (i.e. baryons) is in the form of hot or warm plasma, it emits and absorbs X-ray line radiation that can only be studied using high-resolution X-ray spectroscopy. But even colder gas or dust (i.e. the major tracers for star formation) can be studied through absorption of background X-rays.

After the first pioneering observations with the grating spectrometers of the *Einstein* and *EXOSAT* satellites, the field of high-resolution X-ray spectroscopy became mature through the grating spectrometers on board of *Chandra* and *XMM-Newton* (both launched in 1999). In 2016 the first microcalorimeter spectrum was obtained through the *Hitomi* satellite. This offered the opportunity to study spatially extended sources, in particular with high resolution at high energies. The technique holds great promise for the *Hitomi* successors *XRISM* and ESA's big flagship mission *Athena*.

Still, in the soft X-ray band these new missions have lower energy resolution ($R <$ 200 for oxygen) than the current gratings on *Chandra* and *XMM-Newton*, which have an effective area in this band of 80 cm^2 or less. Despite this, the soft X-ray band below 1.5 keV is actually the richest one in terms of diagnostic power because it contains spectral lines from all metals heavier than boron in all ionisation stages.

There is a large number of important astrophysical questions that need high resolving power in the soft X-ray band, in order to be properly addressed:

- *Where and in what physical state are the Universe's missing baryons, and how does their wandering in-and-out of structures affect the evolution of the Universe and of its different components?*
- *How do winds from Active Galactic Nuclei (AGNs), Supernovae (SNe) and X-ray binaries (XRBs) redistribute metals in their surroundings?*
- *Where are the metals and in which atomic – solid state are they locked?*
- *How do stellar winds affect the chemical composition of exoplanets and the general conditions for the existence of life as we know it?*

While *Athena* will open up the road to the solution of these important problems, by detecting, both in emission and absorption, the densest 20% of the extremely tenuous and diffuse gas that permeates the space between and around galaxies, none of these can be completely addressed without the soft X-ray sensitivity (square root of effective area and resolving power) needed to detect the remaining 80% of this

---

[1]All atoms heavier than hydrogen and helium in the common astronomical use of the word

medium and the resolving power needed to disentangle all its different physical components and study their dynamics. This is key to understand structure formation and their evolution.

In this paper we present these questions in some detail and conclude (Sect. 7) by defining the mission-concept needed to complete *Athena*'s baryon census and address all these questions: a medium-size (according to ESA standard) soft X-ray dispersive spectrometer (*HiReX*) with a resolving power of 5 000–10 000, and an effective area of 1 500–2 000 cm^2 over the 0.2–1.5 keV band. Such a mission in the 2035–2050 timeframe, would not only greatly benefit from its large predecessor *Athena* (which will also define a number of important signposts to be followed up in greater detail by *HiReX*) but would synergetically operate with all the already foreseen ground-based as well as space missions over the entire multi-messenger spectrum.

2 Galaxy-IGM coevolution: physics, kinematics and chemistry of large scale inflows and outflows

During the Universe's childhood (from age $\sim 0.2 - 2$ billion years), most of its baryonic matter, still in an almost primordial composition, permeated the Intergalactic medium (IGM), filling the space between gently forming galaxies, nurturing them and, in turn, receiving heating photons from newly born stars and the first quasars. These baryons imprint a forest of H I Lyman-α absorption lines in the optical spectra of high-z quasars, and this is how we know of their presence, amount, location and physical state (e.g., [1, 2]). At the age of only ~ 2 billion years, however, puberty impetuously bursts in and the Universe's growth became frantic: structures begun growing quickly in size, by devouring material from the surrounding space at higher and higher rates, phagocytising nearby companions, and grouping with close friends.

According to hydro-dynamical simulations for the formation of structures in the Universe (e.g., [3, 4]), this activity was accompanied by a metamorphosis of the tenuous photo-ionised material filling the space between galaxies and feeding their growth: baryons in the IGM were more and more violently pulled towards the growing gravitational potential wells of virialised structures and shrunk into a web of sheets and filaments getting shock-heated to temperatures of $T \simeq 10^5 - 10^7$ K and so becoming virtually invisible in H I absorption. At the same time, freshly metal-enriched baryons started roaming out of galaxy discs, pushed out by powerful supernovae and Active Galactic Nuclei (AGN) winds, wandering into and metal-polluting the circum-galactic medium (CGM) and the surrounding IGM. This cycle of baryons and metals in and out of galaxies proceeded essentially unchanged until our days, and most of the Universe's ordinary matter today should therefore be in a highly ionised state, heavily metal-enriched, and concentrated in the filaments and nodes of the cosmic web.

All this however, has not been observationally verified yet (from which, the so called 'missing-baryon' problem), the main reason being the lack of proper instrumentation in the X-rays. Extreme-UV (to which we are blind because we are located in the disc of the Galaxy) and X-ray photons are those that most efficiently interact

with highly ionised metals, i.e. with the majority of the baryons of the Universe, so that the physics, kinematics and chemistry of these baryons can only be studied through high-resolution X-ray spectrometers, especially in the 0.1–1.5 keV band, where most of the astrophysically abundant elements have their photo-electronic transitions and imprint remarkable emission and absorption lines.

2.1 The intergalactic medium at $z < 2$

The local IGM should be populated with hot baryons with temperatures of about 1 million degrees. At these temperatures, hybridly ionised gas (i.e. shock-heated gas undergoing additional photo-ionisation by the metagalactic radiation field) has only one neutral atom of hydrogen out of ten million and residual opacity due to astrophysically abundant metals. In particular the He-like ion of oxygen is expected to imprint a "savannah" of He-α absorption lines, each with rest-frame equivalent width EW$\lesssim$10 mÅ, in high resolution soft X-ray spectra of background quasars, analogous to the HI Lyman-α forest seen in the optical spectra of quasars at $z > 2$ (e.g., [5]). The strongest of these lines (EW $\sim 10 - 20$ mÅ) are imprinted by the innermost parts of the CGM of large and rare intervening halos, while the weakest and more common lines (EW ~ 1 mÅ) are produced by tenuous intervening filaments of the intergalactic web (e.g., [6, 7]).

The search for the O VII-savannah from the missing hot baryons in the intergalactic medium (the so-called Warm-Hot Intergalactic Medium: WHIM) started about 20 years ago, when the first relatively high resolution X-ray spectrometers became available with NASA's *Chandra* and ESA's *XMM-Newton* observatories. However, after a number of failed attempts and controversial tentative results (e.g., [8, 9], and references therein) it became clear that the resolving power and effective areas of these instruments were just not up to the task and that smart observational strategies (very long exposures of bright, relatively high-z targets, coupled with the identification of WHIM signposts) needed to be put in place.

To date, we can only rely on a couple of possible detections, at locations with dramatically different surrounding galaxy environments [10]. With current instrumentation, and over the next 10 years, carefully selected observing programs can be used to strengthen our confidence in these detections and perhaps add a few more WHIM candidates to the census, but clearly the first breakthrough in this field must await missions like *Athena*, for which one of the science goals is indeed the detection of the missing baryons in a WHIM. However, given its limited spectral resolution in the soft X-ray band (R$\simeq$ 200 at 0.5 keV), *Athena* will only be able to detect 100–200 of the strongest (EW$\gtrsim$5 mÅ) O VII WHIM filaments, which should represent only about 20% of the WHIM baryon mass. Moreover, with its ~ 1500 km s^{-1} resolution at 0.5 keV, *Athena* will not be able to resolve the several expected phases of the IGM web, the kinematics (and thus energetics) of the material inflowing onto galaxies and outflowing from them, temperature and metallicity gradients throughout the probed halos, etc.

To increase the number of IGM hot baryon filaments to thousands and detect ≥ 80% of the WHIM mass, to study the physics, kinematics and chemistry of these baryons in details and so understand the IGM-galaxy co-evolution with cosmic

time, a much higher resolution soft X-ray spectrometer is needed, with a resolving power sufficient to resolve thermal (and therefore also turbulent) velocities of light metals in gas with temperatures of $\sim 10^6$ K.

Figure 1 shows two distinct regions of the 100 Mpc^3 periodic box Eagle simulation [4, 12]. These two Eagle regions are dramatically different in galaxy environment and IGM properties, and have been chosen to show the vast range of physical, kinematical and chemical conditions predicted for the local hot IGM depending on the amount of feedback that different regions of the Universe undergo. The insert of Fig. 1a (left panel) shows *HiReX* (red and blue histograms) and *Athena/X-IFU* (green and cyan histograms) mock spectra of two strong and multi-component O VII (top panel) and O VIII (bottom panel) absorbers, spanning a range in rest-frame velocity $v_{rf} \simeq 50 - 800$ km s^{-1}. The total EWs are $49.5^{+2.6}_{-0.6}$ mÅ for O VII and 24.6 ± 0.9 mÅ for O VIII as measured with *HiReX* in only 100 ks. These complex absorbers are clearly associated with the hot gas permeating the largest halo present along this line of sight ($M_{200c} = 2.8 \times 10^{13}$ M$_\odot$), with a rest-frame (Hubble-flow plus peculiar) velocity $v_{rf}^{Halo} \simeq 470$ km s^{-1} and a line of sight impact parameter of only 61 kpc. The *Athena/X-IFU* will detect both the O VII and O VIII absorbers, but only an instrument like *HiReX* would allow us to **unambiguously resolve their multi-component nature and precisely measure temperature and density gradients** across the ~ 750 km s^{-1} broad O VII He-α and O VIII Lyman-α opacity profiles, thus enabling a line-of-sight tomography of the hot halo medium.
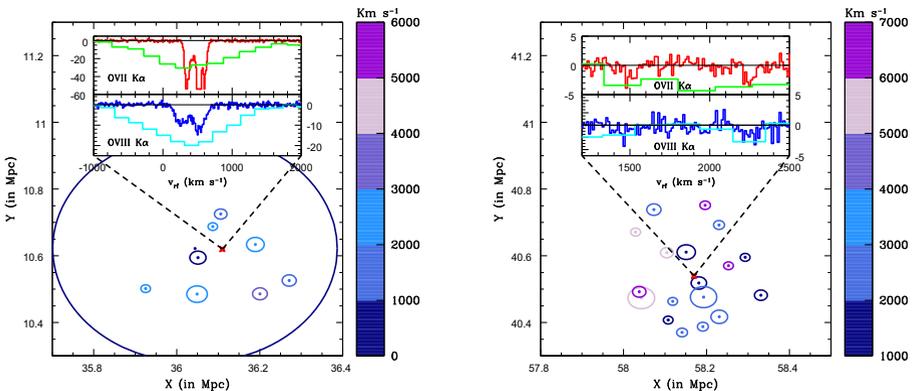

Fig. 1 Two distinct regions extracted from the 100 Mpc^3 periodic box Eagle simulation. The boxes start at $z = 0.10064$ (rest-frame velocity $v_{rf} = 0$) and extend to Hubble-flow distances $v_{rf} = 6770$ km s^{-1} (the size of the periodic box). Circles are all the halos with comoving $M_{200} \geq 10^9$ M$_\odot$ and within 200 comoving kpc from the the lines of sight present in the simulations. Circles have radius equal to half the halo's virial radius in comoving kpc and are color-coded in rest-frame velocity (i.e. redshift) according to the bar-legend to the right of the figures. The inserts in the two panels are small portions of mock *HiReX* (red and blue histograms) and *Athena/X-IFU* (green and cyan histograms) spectra of the two lines of sight (red crosses near the centre of the boxes), centred on the O VII He-α (top panels) and O VIII Lyman-α (bottom panels) transitions at the redshifts of the hot intervening absorbers present in these two boxes. Mock spectra have been produced with the fitting-package *Sherpa* [11] adopting a model consisting of the $\Gamma = 2$ power-law continuum of a bright ($F_{0.2-1.35\,keV} = 10^{-11}$ erg s^{-1} cm^{-2}) background AGN times the opacity to the metal transition produced by the gas in the simulation boxes, and integrating for 100 ks (left panel) and 1 Ms (right panel)

It is worth mentioning that there is also great synergetic potential of *HiReX* and imaging X-ray observatories featuring high effective area and equipped with micro-calorimeters (e.g. *Athena*) thanks to their capability to detect WHIM in extended diffuse emission in oxygen lines (boosted by resonant scattering of the cosmic X-ray background). Combining high-resolution absorption-line studies by *HiReX* with such data will allow determining the physical state of the WHIM gas, e.g. ***differentiate truly a diffuse medium of small overdensity from denser clumps having low filling factor*** (see, e.g., [13, 14]).

Fig. 1 (right panel) shows a dramatically different case. Two much weaker O VII and O VIII absorbers are present along this line of sight, at rest-frame velocities $v_{\rm rf}^1 \simeq 1450 - 1550$ km s^{-1} and $v_{\rm rf}^2 \simeq 2150 - 2350$ km s^{-1}. Their EWs, as measured with *HiReX* in 1 Ms (red and blue histograms), are for component 1: $0.50^{+0.11}_{-0.09}$ mÅ (5.4σ, O VII), $0.37^{+0.11}_{-0.10}$ mÅ (3.7σ, O VIII) and for component 2: $0.60^{+0.09}_{-0.09}$ mÅ (6.4σ, O VII), $0.46^{+0.09}_{-0.11}$ mÅ (4.2σ, O VIII).

Absorber 1 is produced by the outskirts (impact parameter of 0.7 virial radius) of the CGM of a small halo with M$_{200c}$ = 4.6×10^9 M$_\odot$ and rest-frame (Hubble-flow plus peculiar) velocity $v_{\rm rf}^{\rm halo}$ = 1500 km s^{-1}. Absorber 2, instead, is not clearly (i.e. with similar $v_{\rm rf}$) associated with the CGM (or CGM's outskirts) of any halo in the box, and is therefore imprinted by a truly diffuse intervening WHIM filament with its external parts hotter than the centre (compare the symmetrically broader profile of the O VIII Lyman-α absorber to the narrower profile of the O VII He-α absorber). The *Athena/X-IFU* (green and cyan histograms) does not resolve the two absorbers and detects only the sum of the two O VII (not O VIII) lines, thus not allowing for a clear halo association.

This wealth of diagnostics can only be achieved with soft X-ray resolving powers $R \gtrsim 5000$.

2.2 The circum-galactic medium

2.2.1 The CGM of the Milky Way

Despite many obstacles, the Milky Way is still one of the best laboratories to test our understanding of galaxy formation and evolution. High resolution X-ray spectroscopy is essential in addressing several outstanding important questions in this field. The hot phase of the CGM can only be probed via spectroscopic features from highly ionised metal species such as O VII and O VIII. The soft X-ray band between 0.2–2 keV also offers a unique opportunity to probe the cold, warm, and hot phases of the Milky Way CGM simultaneously, and therefore provides a complete census of the baryon content of the Milky Way. *Athena* [15] will detect absorption lines with EWs greater than 5 mÅ near the strong lines of O VII and O VIII but with poor velocity information. On the other hand, with its high sensitivity ($A_{\rm eff}$ ~1 500–2 000 cm^{-2}) and high spectral resolution (R ~ 10 000), *HiReX* will be able to provide detailed information on the physical, kinematic, and chemical status on the Milky Way CGM at a level that cannot be addressed by *Athena*.

Baryonic content of the Milky Way Recent studies suggested that a large amount of the baryons in the Milky Way is missing (e.g., [16, 17]). These missing baryons are either located in the distant hot halo or dispersed in the local large-scale structure via some feedback processes (e.g., [18–21]). However, the fate of these baryons is very difficult to determine with the current generation of X-ray telescopes because: (1) the coupling with the Doppler-b (line width) parameter leads to large uncertainties in the column density measurements of ion species such as O VII and O VIII; (2) we lack the information of the ionisation state as well as the chemical abundance of the CGM. The decoupling of the Doppler-b parameter and the column density can be achieved by measuring high-order transitions such as the O VII Heβ line, which so far can only be done with two or three very high S/N sight lines toward background AGNs. However, *HiReX* is more than 1 000 times more sensitive than the current generation X-ray spectrometers, and it will allow us to obtain an accurate measurement of ion column densities for more than 100 AGN sight lines. Furthermore, with the high spectral resolution, *HiReX* can clearly detect and resolve nearly all the ionisation stages of oxygen from O I to O VIII, as well as several other ion species. This allows for *a precise determination of the ionisation mechanism, and the relative abundance of the metals*. With this information, we expect a complete understanding of the fate of the missing baryons in our Milky Way galaxy.

Kinematic, physics and chemistry of the Milky Way CGM By providing velocity information, high resolution spectroscopy is critical in diagnosing the physical, kinematic, and chemical states of the Milky Way CGM. With velocity information, we can find out *whether the X-ray absorbing gas is in a state of rotation/inflow/outflow, resolve the absorption lines into different components, and distinguish between thermal and turbulent line broadening.* A resolution of $R \sim 5\,000 - 10\,000$ can help match physically distinct phases and measure bulk velocity better than $\sim$5–10 km s^{-1} (based on the line centroid) and measure the Doppler-b parameter to better than $\sim$10–20 km s^{-1} (based on line width). Such resolution is necessary to resolve line profiles and so, for example, discriminate between a rotating and non-rotating hot halo (vital for understanding the accretion and feedback history of the Galaxy; Fig. 2), separate different line transitions (e.g., O II Kβ from O VI Kα, and O II Kα from O$_2$ Kα), resolve bulk velocity for C, O, and Fe, and resolve turbulent from thermal motion at $T < 10^7$ K. This is a critical advantage of *HiReX* over *Athena* as the latter, with a resolution of $R \sim 200$, can detect lines without being able to resolve them.

2.2.2 The CGM of external galaxies

Athena will likely detect extended hot halo gas around $L_\star$ [24, or Schechter Luminosity,] galaxies to about 100 kpc (according to models; [25]) but with poor velocity information. These hot halos are likely to extend far beyond 100 kpc (250–500 kpc; Fig. 1), based on models (e.g., [4]) as well as the observations of stacked Sunyaev-Zeldovich measurements (e.g., [26]). The extent of the hot gas, as well as its mass, composition, and temperature are set by the accretion and feedback processes, which are poorly constrained. These fundamental properties will be determined by the
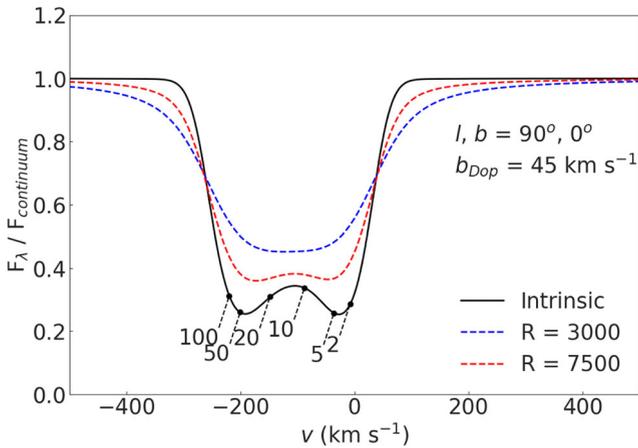
Fig. 2 The O VII Heα absorption line from a rotating Galactic hot halo [22], modeled with $v_\phi = 180$ km s^{-1}, toward $l = 90°$, $b = 0°$, with Doppler parameter $b = 45$ km s^{-1} [23]. The contributions as a function of distance from the Sun are shown along the bottom of the intrinsic curve, in kpc. The rotation curve of the hot halo, which is encoded in the line shape, can be determined from high spectral resolution observations

HiReX spectroscopic mission, providing great advances in our understanding of galaxy formation and evolution.

Missing metals and baryons in external galaxies The optical parts of galaxies and their gaseous discs are missing about 75% of the metals produced by their stars and 70-90% of the initial baryon content [17, 27]. The inner 100 kpc around galaxies will be probed with *Athena*, but the gas and metal masses increase with radius, so most of the baryons and metals lie beyond 100 kpc. These outer regions will be studied with *HiReX*, which has a sensitivity about an order of magnitude better than *Athena* for line detections. It will measure absorption in more than 100 galaxy halos, providing an excellent radial profile of ions (probably to 250–500 kpc, 1–2R$_{200}$) in the long-lived halo where the cooling time exceeds a Hubble time. The O VII columns can be estimated from an extrapolation of Milky Way gas and from direct detection along one extragalactic sight line [10, 25]. These O VII columns are more than an order of magnitude greater than observed UV O VI sight lines [28, 29] from cooler gas (also true for lower ionisation state lines), so these X-ray absorption lines will yield *a definitive measure of the metals, determining whether the missing metals lie within an extended hot halo.* This relates directly to the formation and evolution of galaxies.

Single lines of sight will detect only a few lines (He-like and H-like C and O), but by stacking the absorption systems, weaker lines will be revealed. These include higher ionisation lines than O VII, such as O VIII, Ne IX, and Ne X, additional lines at the typical ambient temperature of the halo, such as N VI, N VII, as well as lower ionisation state lines, such as O I, O III, O IV, and O V. These lines will define the temperature distribution of ions, which is caused by cooling and feedback processes and has become an important prediction of models.

Feedback and rotation in external galaxies Feedback from SNe and AGNs regulates the formation of galaxies and their environment. Detailed measurements of the hot X-ray gas provide a snapshot of the feedback today. Feedback will cause the outflow of gas from the disc and there will be turbulence caused by these motions (e.g., [30]). The net effect will be to broaden the lines beyond the thermal widths (40–50 $km\,s^{-1}$), and *HiReX* will have the velocity resolution to separate a line into its thermal and turbulent components, the latter being a direct measure of feedback.

A nascent galaxy gains angular momentum from surrounding non-uniform regions, with the rotational velocity increasing as the gas flows to smaller radii [31]. This leads us to expect the hot halo to be rotating, although the initial value of the specific angular momentum can be decreased by the accretion of other halos, and if feedback is very effective, it will mix the angular momentum of the hot halo gas. Thus the rotational profile of the hot halo contains vital clues about accretion and feedback. *HiReX* will measure the velocity of line centroids to exceptional accuracy (<30 $km\,s^{-1}$) for sight lines through many different galaxy halos, allowing one ***to assemble a composite rotation curve to several hundred kpc.***

2.3 Outskirts of clusters and groups of galaxies

Clusters and groups of galaxies represent unique signposts in the Universe where both thermo- and chemo-dynamical properties of the diffuse ionised plasma can be studied in detail through X-ray observations. The past (*ASCA* and *Beppo-SAX*) and the current generation (*XMM-Newton*, *Chandra* and *Suzaku*) of X-ray satellites have demonstrated that metals are not homogeneously distributed in the intra-cluster medium (ICM; see [34, 35] for recent reviews on results from simulations and observations). Indeed, relaxed cool-core clusters are characterised by negative metallicity gradients, with an enhanced metallicity in the core regions, likely to be associated to the process of star formation of the galaxies whose assembly gave rise to the Brightest Cluster Galaxies (BCGs) that are at the centre of these clusters. On the other hand, dynamically disturbed non–cool core clusters have a much flatter metallicity gradient, with a lower level of enrichment in central regions. The reason for this is due to the mixing of the gas due to the same dynamical processes which lead to the disruption of the cool core. While these observational results hold out to about one quarter of the virial radius, R_{vir}, the situation is less clear at larger radii, where reliable measurements of metallicity are hampered by the low level of emissivity and the corresponding need for precisely characterising background contamination. Indeed, the low particle background of the *Suzaku* satellite recently allowed to trace, although with rather large uncertainties, the ICM metallicity out to scales approaching the virial radius of a handful of nearby clusters (see Fig. 3).

These studies gave a clear indication of the inextricable link between the recent dynamical history of galaxy clusters and the pattern of chemical enrichment within regions of galaxy clusters and groups which encompass a fraction of their virial region.

Quite interestingly, cosmological hydrodynamic simulations that include a detailed description of chemical enrichment converge to indicate that a negative metallicity gradient in the central regions of galaxy clusters and groups naturally
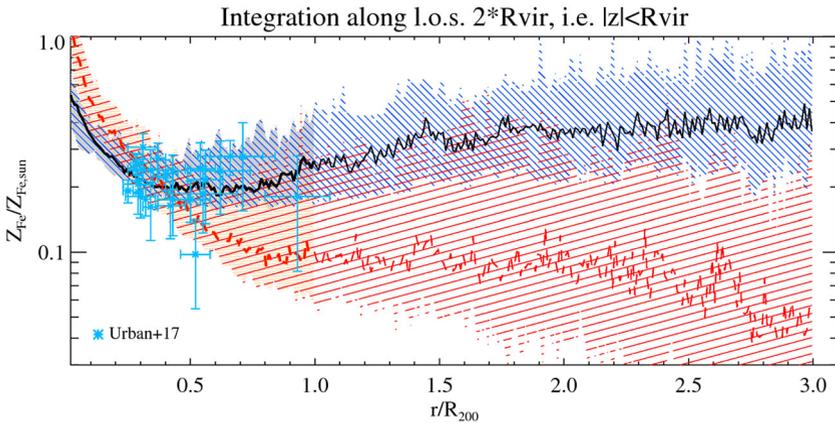
Fig. 3 Comparison between observed metallicity profiles in the outskirts of galaxy clusters and results from cosmological hydrodynamic simulations. The cyan asterisks with errorbars correspond to the observational results by [32] for 10 nearby clusters observed with *Suzaku*. Simulation results corresponds to the set of simulated clusters whose metallicity profiles have been studied in [33], with blue and red corresponding to simulations that include and exclude the effect of AGN feedback, respectively. The two curves correspond to the median profile computed within the simulation set, while the shaded areas mark the corresponding r.m.s. scatter

arises as the result of the processes of star formation and hierarchical assembly of such structures, independent of the efficiency and nature of the sources of energy feedback that should regulate star formation. On the other hand, the same simulations also predicted that largely different patterns of chemical enrichment are expected in the outer regions of galaxy clusters when including different feedback sources: while feedback from supernovae generates a negative metallicity gradient extending out to the virial radius and beyond, the inclusion of AGN feedback causes a flattening of the metallicity profiles beyond about half of $R_{\rm vir}$ (e.g., [36, 37]). In fact, this different behaviour is due to the efficiency with which AGN feedback expels metal-enriched gas from the CGM of the proto-cluster galaxies at redshift $z \simeq 2$–4, when gas accretion onto SMBHs reaches the peak of activity. This causes in turn a pre-enrichment of the IGM, which leads to a sort of metallicity floor at low redshift (e.g., [33]). This effect is illustrated in Fig. 3, which shows the metallicity profiles predicted by simulations both including (red) and excluding (blue) the effect of AGN feedback, and compares them to observational data on ICM metal enrichment out to the largest radii sampled so far.

While the much higher sensitivity and spectral resolution of *Athena/X-IFU* are expected to significantly improve with respect to the current observations out to R_{500} [38], mapping the metallicity of the ICM in emission beyond $R_{\rm vir}$ could become prohibitively expensive, or even hardly possible, due to the requirements on the background control and collecting area.

At the same time, while current observations of cluster outskirts mainly trace Fe (by mainly measuring the equivalent width of lines in the Fe-K complex), tracing different chemical species would provide further insights on the processes of feedback and gas circulation that determine the cosmic cycle of baryons in general. For

instance, Fe and O are expected to be produced by different stellar populations, which are characterised by different lifetimes and, therefore, release them over different time-scales. As a consequence, their distribution could differ, depending on the efficiency of the dynamical processes (e.g. outflow, turbulence) driving their diffusion [39].

Figure 4 compares the O VII, O VIII and Ne X absorbing systems predicted by the cooling-star formation-supernova feedback (CSF) and AGN feedback (BH) simulations [33]. As expected, in the BH simulation that involves redistribution of metals by AGN feedback over cluster outskirts, the absorption lines are much more prominent. The lines are resolved and can be used to study the flow of metals in the cluster periphery. Note, that the higher temperature than in the WHIM leads to stronger lines of O VIII and Ne X. This property can be used to separate the WHIM contribution from the hotter cluster outskirts.

High spectral resolution (10–50 times better than calorimeters) absorption tomographic studies of cluster gas allow us *to trace different elements at different*
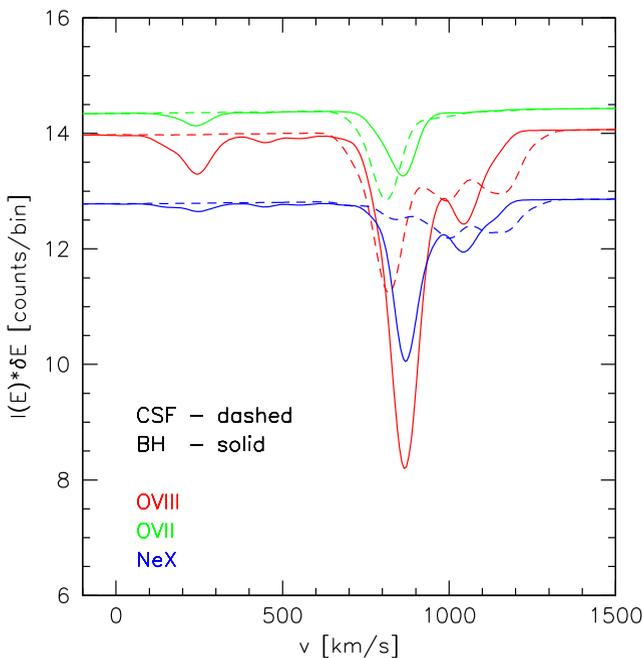

Fig. 4 Velocity profile of the absorption lines produced by O VII, O VIII and Ne X ions in the spectrum of a background AGN at a projected distance of ∼1.6 Mpc from the centre of a massive cluster from simulations of [33]. Compared to WHIM, the role of O VIII and Ne X is enhanced due to the higher temperature of the gas. The dashed and solid lines correspond to the CSF and BH runs, correspondingly. Two prominent absorption structures are present for this sight-line, one at +900 km s^{-1} and a fainter one at +300 km s^{-1}. Each structure possesses an additional kinematic substructure on top of the thermal broadening. As expected, the lines are significantly stronger in the BH run. The vertical axis shows the number of counts per resolution element for the AGN with 0.5–2 keV flux ∼ 2 10^{-13} erg s^{-1} cm^{-2} and photon index $\Gamma = 1.2$ for a 1 Ms observation with 1500 cm^2 effective area

ionisation stages, and to measure their spatial distribution and motion along the line-of-sight at large radii (out to $2R_{vir}$) that are impossible to do in emission.

2.4 AGN and galactic outflows

Current X-ray observatories have established the presence of outflows, produced in the vicinity of supermassive black holes (SMBH) at the heart of AGN. The so-called warm absorbers are detected in a large number of AGN via a wealth of soft X-ray absorption lines from C, N, O, Ne, Mg, Si and S, tracing low ionisation gas outflowing at 100s to 1000s of $km\,s^{-1}$ and located at a few 10s–100s of parsecs from the SMBH [40–42]. In obscured Seyfert galaxies, this medium is observed via the presence of numerous soft X-ray emission lines. The temperature, density and the source of the ionisation equilibrium of the emitting gas can be measured from radiative recombination continua (RRC) and He-like triplets, as well as from a full characterisation of satellite lines and the Fe L 'forest' [43, 44].

There is increasing evidence for the presence of blue-shifted Fe K-shell absorption lines in AGN at rest-frame energies higher than 7 keV [45, 46]. These so called ultra fast outflows ("UFOs") are likely driven off the accretion disc by either radiation pressure [47] or magneto-rotational forces [48, 49], or both, and the outflow rates derived can be large, of order several solar masses per year. Furthermore these fast, energetic winds, may be the initial stage of the sweeping process that leads to mass losses of hundreds to thousands of $M_{\odot}\,yr^{-1}$ on the scale of the AGN host galaxy [50, 51]. The presence of soft X-ray absorption lines from UFOs has been detected too, showing that these fast winds exhibit different ionisation states [52–56]. These arise from He and H-like O, Ne and L-shell Fe lines and are most apparent when the spectrum is more absorbed overall. This may be associated with lower ionisation gas, like the Broad Absorption Line (BAL) winds in the UV, as part of a clumpy phase of the disc wind capable of producing substantial X-ray obscuration [57, e.g., NGC 3783,]. This process can then facilitate radiative acceleration and driving of winds in powerful quasars at higher redshifts, which are currently beyond reach for soft X-ray spectroscopy.

It is essential to measure all these wind phases over a wide range of radial distances and velocities to understand their nature, their link, their launching mechanism(s) and duty cycle, and thus, ultimately, their relevance in polluting the host galaxy's surroundings with metals, as predicted by simulations (e.g. Sections 2.1–2.3, Fig. 3). This can only be performed via accurate measurements of the wind physical properties (e.g., column density, density, ionisation parameter, velocity, distance, time variability) and their relationships, which, in turn, requires high spectral resolution and throughput in the soft X-rays. High resolving power R∼5 000–10 000 is also critical for an *accurate determination of the total wind kinetic power required for galaxy feedback*. The X-ray wind energetics can then be compared to that of larger scale molecular and ionised outflows to assess their efficiency in driving (via either energy or momentum) feedback on galaxy scales [58]. A soft X-ray grating with the parameters of *HiReX* (Section 7) is also required to robustly measure wind variability in order to deduce its characteristics.

The nearby QSO, PG 1211+143 (at $z = 0.0809$) has one of the prototype ultra fast outflows at soft X-rays. The current *XMM-Newton RGS* and *Chandra HETGS* grating observations have a combined total exposure exceeding 1 Ms [53, 54]. However, the line diagnostics are currently limited to the strongest $1s \rightarrow 2p$ lines, due to the low effective area and resolution, while the mechanism for the outflow variability is uncertain. High throughput and resolution at soft X-rays are prerequisite for measuring absorber variability. Figure 5 (left panel) shows a *HiReX* simulation of a short 20 ks (typical variability timescale of AGN in the X-rays) time-slice of PG 1211+143, focused on the O VII line series, demonstrating that the wind variability can be accurately measured on these short timescales. The strongest line profiles (e.g. O VIII $1s \rightarrow 2p$ and O VII $1s \rightarrow 3p$) are saturated, providing a direct measure of the gas covering fraction, to within $60 \pm 5\%$. Variations in covering could correspond to the transverse motion of outflowing clouds across the line of sight on dynamical size-scales of a few gravitational radii. The weaker higher order absorption lines are not saturated and yield an accurate measure of the hydrogen equivalent column density to within $N_H = 2.9 \pm 0.2 \times 10^{21}$ cm^{-2}. Changes in ionisation in response to a decrease in the X-ray continuum, via recombination, can also be measured to an accuracy of $\pm 5\%$ on a 20 ks timescale. Such monitoring enables ***the density, location and size scale of the absorber*** to be directly measured (e.g., [59]). The data would also allow us to determine the outflow properties, such as the column, covering and ionisation, as a function of the wind velocity. The wind energetics can then be robustly assessed.

The second example is of the Seyfert 1 galaxy, NGC 5548 (at $z = 0.017175$). This AGN has a notable outflow, spanning at least an order of magnitude in outflow velocity and two orders in ionisation [60]. Presently these outflow components can only be resolved in velocity space through high resolution UV spectroscopy, but not in X-rays; e.g. neither at the resolution of the current X-ray gratings on-board *XMM-Newton* or *Chandra*, nor, in ten years from now, with *Athena* below 1 keV.
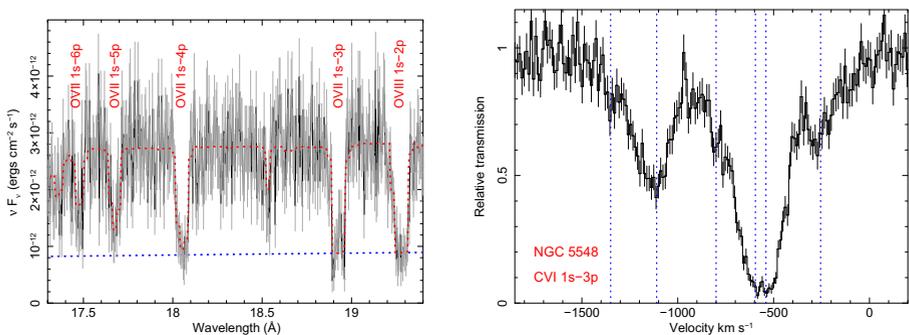

Fig. 5 Left – simulations of a 20 ks time slice of the variable, fast outflow in PG 1211+143, with a resolution of $R = 5000$. The higher order absorption O VII line series is seen in PG 1211+143, where the strongest saturated lines reveal the covering fraction and the higher order lines determine the column density. Right – a 120 ks simulation of the Seyfert 1 galaxy, NGC 5548, at a resolution of $R = 10000$, showing the wind profile in C VI. The wind can be resolved into at least five distinct velocity components (vertical dashed lines), enabling the wind properties, such as its ionisation, to be mapped as a function of the outflow velocity. A turbulent velocity of $\sigma = 70$ km s^{-1} was adopted

Figure 5 (right) shows a 120 ks simulation of the outflow in NGC 5548, based on its unobscured X-ray state. For illustration, the velocity profile at the C VI $1s \rightarrow 3p$ line is plotted, where a resolution of $R = 10000$ will fully resolve all the wind components. In this example at least five distinct velocity components are resolved, with $v = 250, 550, 800, 1100, 1350 \, \text{km s}^{-1}$, each measured to a typical accuracy of $\pm 10 \, \text{km s}^{-1}$. Furthermore the wind may vary in ionisation as a function of velocity, e.g. as can occur if the highest ionisation gas originates from the fastest wind components. The high resolution X-ray spectrum would make it possible *to measure all the wind properties well beyond those measurable in the narrow ionization windows offered by UV spectroscopy, such as ionisation, as a function of the outflow velocity, providing a multi-dimensional map of the wind and ultimately revealing its complete physical structure*.

3 The inter-stellar medium

3.1 Chemical composition and dynamical structure of the ISM

The diffuse interstellar medium (ISM) has a crucial role in the evolution of the Galaxy. Different elements are produced by various types of stellar phenomena (e.g. supernovae type Ia, core-collapse and AGB winds) and their abundances are the direct testimony of the history of stellar evolution. In the neutral phase, heavy elements like iron, calcium, magnesium, etc. are mostly locked into solids and depleted from the gas phase. However, the interstellar dust composition is not well known and the total (gas + molecules + dust) abundances are yet to be accurately determined. At long wavelengths, for instance, it is still challenging to distinguish between carbonaceous and silicate dust grains (e.g., [61], for the 10μm feature).

The soft X-ray energy band (~ 0.2–2 keV) contains the strongest transitions of the K shell from the most abundant interstellar atomic species (C, N, O, Ne, Mg, Si) and the Fe L shell. Dust and molecules also imprint a forest of spectral features in the form of X-ray absorption fine structures (XAFS) supporting multi-wavelength studies of interstellar phases and synergies. It is possible to probe the ISM complex composition through the study of interstellar absorption features in the high-resolution X-ray spectra of background galactic X-ray binaries and active galactic nuclei.

High-quality grating spectra unambiguously show the presence of interstellar absorption lines and edges in every spectrum. The whole series of oxygen (O I-VIII), N I-II, Fe I L_2 and L_3 edges, Ne I-X, and many more species are found (e.g., [62–64]). Strong evidence of dust and molecules in the form of complex XAFS was found in the absorption edges of elements like O, Mg, Si and Fe that are significantly depleted from the gaseous phase (e.g., [65–67]). Between 15–25% and 65–90% of the total amount of O I and Fe I (and possibly higher fractions for Mg I and Si I) could be locked in dust grains [68–71]. Solids may therefore be a significant reservoir of metals and provide a solution to the problem of the missing oxygen, but the uncertainties in the atomic databases and the limited spectral resolution of current detectors ($R \sim 300$–500 for *RGS* and *LETGS*) undermine the detection and measurements of

dust features (see, e.g., [72, 73]). A next-generation detector with superior effective area ($A > 1000\,\text{cm}^2$) and spectral resolution ($R > 1000$) at $E \lesssim 1.5$ keV is necessary *to resolve each individual absorption line from the dominant ions and dust compounds.*

Micro-calorimeters, like *Athena/X-IFU* and *XRISM Resolve*, will have $R < 200$ at $E = 0.5$ keV and thus cannot serve this particular scope. Wavelength-dispersive grating spectrometers are needed. Here we adopt a grating-spectrometer (*HiReX*) with $R = 5000$ resolving power and $2000\,\text{cm}^{-2}$ effective area at the Fe L and O K edges (e.g., [74]).

We use as template the best fit model for the *RGS* stacked spectrum of Cygnus X-2 which includes a comprehensive description of the ISM (neutral and ionised gas plus dust). The dust mainly consists of pyroxene (MgSiO$_3$), metallic iron and fayalite (Fe$_2$SiO$_4$). We have simulated a Cygnus X-2 high-resolution spectrum with an exposure time of 50 ks (see Fig. 6).

All the relevant absorption features are well resolved, even the O III doublet at 23.05–23.1 Å. The accuracy on the column densities of each molecular compound would be around a few % or better. The uncertainties on the velocities of each gas component will be less than few $\text{km}\,\text{s}^{-1}$, providing for the first time *accurate measurements on both line widths and line of sight velocities*. With the current detectors we can only get upper limits of about 100–200 $\text{km}\,\text{s}^{-1}$. Neither *RGS* nor *Athena X-IFU* are able to resolve and distinguish the individual features. The uncertainties on
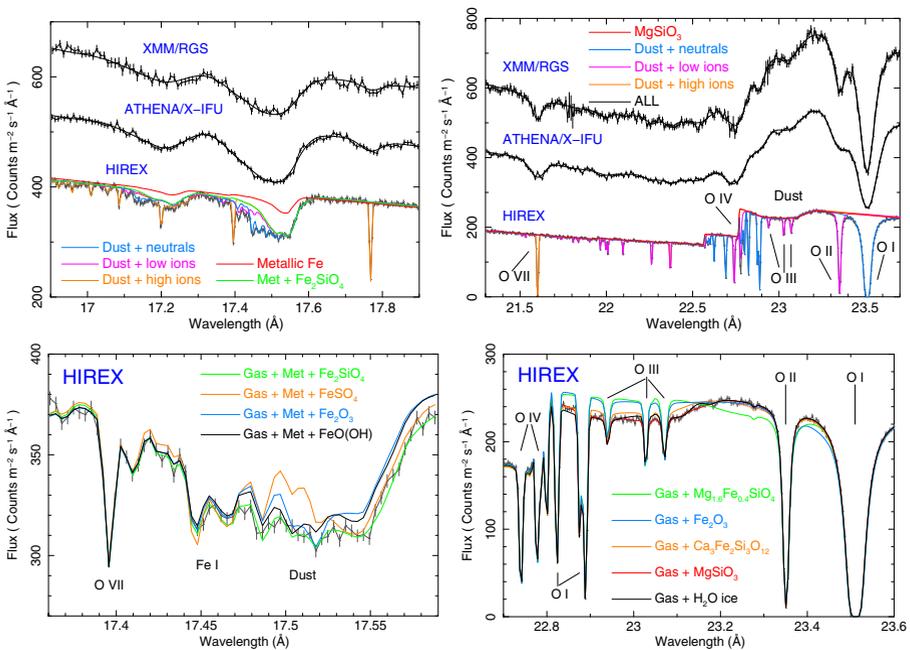

Fig. 6 Cygnus X-2 *HiReX* 50 ks spectrum simulated using the *RGS* fit model as compared to *Athena/X-IFU* and *XMM-Newton/RGS* (top panel), which are shifted along the Y-axis for displaying purposes. Low ions refer to e.g. O I-V and high ions to O VI-VIII. Only *HiReX* will be able to resolve individual lines

gas column densities and temperatures will be better than 5%, enough to distinguish between photoionisation and collisional equilibrium.

Similar studies will be possible on the ISM of nearby galaxies, by using local X-ray binaries or Ultra-Luminous X-ray sources (ULXs) as beacons, and on the ISM of distant galaxies by observing GRB X-ray afterglows soon after the prompt emission and during their fading phase.

4 Metals in-and-around stars

4.1 Stars

To constrain the metal processing operated by stars the understanding of stellar formation and evolution, for both high- and low-mass stars, needs to be improved.

High-mass stars are crucial for a wide range of astrophysical aspects: the starburst events, the chemical enrichment of the Universe, and the multi-messenger astronomy via gravitational wave (GW) events. These stars have a strong impact on their Galactic environment through their winds and explosions as supernovae. When in binaries, they are the progenitors of double-compact systems which finally merge, emitting GWs. Soft X-rays in massive stars arise in shocks linked to their winds (e.g. [75]). X-ray line morphologies are sensitive probes of the properties of these winds (e.g. [76]), providing crucial information on many aspects of these outflows. The limited sensitivity of existing facilities and the limited spectral resolution in the soft X-ray domain of forthcoming calorimeters are insufficient to resolve these lines and to study their temporal evolution. A high-resolution and high-efficiency spectrometer in soft X-rays will not only help constrain the mass-loss rates of massive stars, but will allow ***tracing the impact of small and large-scale wind structures***. Doppler tomography of resolved X-ray lines will ***map the plasma in the co-rotating magnetosphere*** of magnetic massive stars. The proposed mission will further allow studying the propagation of photospheric pulsations throughout the stellar wind, investigating the formation of radiative recombination continua, and constraining the fraction of the stellar wind that is under the form of plasma.

Low-mass stars are the most common and longest living stars. Their evolution is substantially affected by their exchange of mass and angular momentum with their ambient medium during their life. During their formation, low-mass stars accrete mass from their circumstellar disc via magnetically channelled streams. At the stream footpoints, the accreting material impacts with the stellar atmosphere producing shocked plasma at ~ 3 MK. The current generation of X-ray spectrometers demonstrated that soft X-rays are a powerful probe of the shock region [75, e.g.]. The shocked plasma is expected to move inward with $v \sim 100 \, \mathrm{km \, s^{-1}}$. The rotational monitoring of its line-of-sight velocity would tightly constrain the accretion geometry. The limited spectral resolution in soft X-rays of calorimeters will prevent these kind of studies. Conversely, the proposed mission concept will allow ***to systematically measure the shocked-plasma velocity*** [78, this measure is nowadays achievable only for the nearest young accreting star TW Hya,], and to perform ***Doppler-imaging of the shocked plasma on the stellar surface*** for the nearest sources (Fig. 7). This
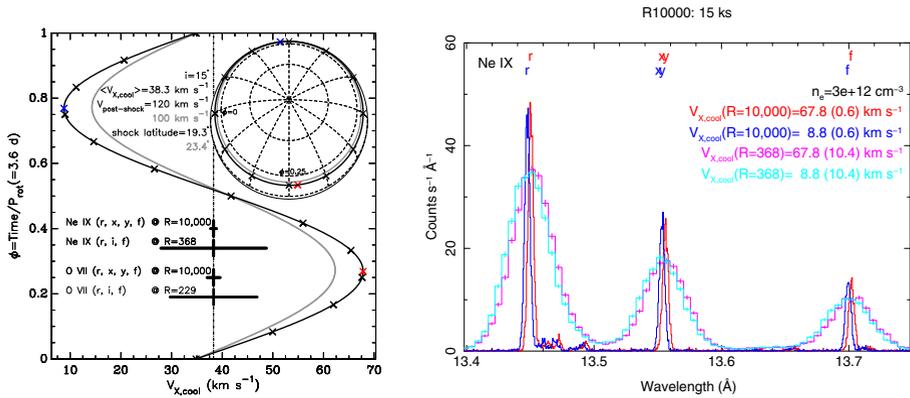
Fig. 7 Kinematics of a point-like accretion-shock at the surface of the young accreting star TW Hya. Left panel: predicted stellar rotational-phase vs. line-of-sight velocity of shocked-plasma at the accretion-stream base. The top-right insert displays the phase-dependent shock position on the sky-projected stellar photosphere. Right panel: simulated X-ray spectra of the Ne IX He-like triplet with a very high-resolution high-effective area soft X-ray spectrometer ($\Delta\phi=0.05$, corresponding to 15 ks), compared to Athena X-IFU [77]. The rms errors on the velocity fitted value (estimated from 500 simulated spectra) are provided between parentheses and as horizontal error-bars in the left panel

X-ray tomography of the extended shocked emission will be valuable for comparison with the results of Zeemann-Doppler imaging of stellar photospheres [79]. In addition, the *HiReX* mission concept will allow to resolve line widths, and hence to constrain the turbulent motions in the post-shock region.

When accretion ends, low-mass stars enduringly lose mass and angular momentum via stellar winds and coronal mass ejections (see Section 4.2). These phenomena are governed by the stellar magnetic activity, that is best studied by probing coronal phenomena in X-rays. Flares are the main manifestation of energy transfer from the magnetic field to the coronal plasma. Studying the motions of plasma within flaring structures is important to constrain flare physics, and improve coronal modelling. Plasma located near the flaring loop footpoints (where $T \sim 10\,\mathrm{MK}$ and the emission measure is maximum) is expected to move with $v \sim 100$–$500\,\mathrm{km\,s^{-1}}$. Such motions, almost unexplored nowadays in stars, can be systematically studied with *HiReX* by *monitoring the evolution of line profiles during stellar flares.* *Athena/X-IFU* will likely allow to monitor line shifts (without yet resolving line profiles) only in the extreme cases of very hot flares occurring in extremely active stars.

4.2 Planets

4.2.1 Exoplanet energetic photon radiation environments

The rate at which gas is lost from an exoplanet's atmosphere is critical for the survivability of surface water. Atmospheric mass loss can be driven by both thermal and non-thermal processes, which depend upon the radiation and winds of their host stars. The dominant thermal process is hydrodynamical outflow energised by extreme

ultraviolet (EUV; 100–912 Å) and X-radiation (0.1–100 Å) that heats the exoplanet's thermosphere and levitates gas against the exoplanet's gravitational potential (e.g., [80]).

Most of the thermospheric heating is by EUV photons but this radiation cannot be observed directly because of interstellar H absorption. The chromospheric UV and FUV are inadequate EUV proxies. The strength and spectral energy distribution of a star's EUV emission instead arises from the transition region and corona. The 30–60 Å range contains many lines from the same ionisation stages. ***Observing these soft X-ray lines enables prediction of the EUV spectrum and thereby constrains the atmospheric mass loss.***

Detecting the relevant lines in exoplanet hosts requires very sensitive high-resolution ($R \geq 5\,000$) spectroscopy that is not feasible with any existing or planned future missions, including *Chandra*, *XMM-Newton* or *Athena*. Observations through flares and other stochastic variability are also required to understand how EUV fluxes vary in time.

4.2.2 Stellar winds coronal mass ejections and exoplanet atmospheric loss

The flow of ionised stellar wind electrons and protons erode an exoplanet's atmosphere, while coronal mass ejections can enhance the loss rate by an order of magnitude or more [81–84]. Recent measurements by the MAVEN satellite [85] confirmed that the primary mass-loss mechanism for water on Mars is erosion by the solar wind.

The wind mass loss rates for late-type dwarfs are notoriously difficult to measure as the solar mass-loss rate is only about $1.5 \times 10^{-14} M_{\odot}$ yr^{-1}. Radio observations yield only upper limits and the few indirect estimates possible based on Lyα absorption in the "wall" of hydrogen at the stellar analogy of the heliopause [86] are prone to modelling and systematic uncertainty.

Charge-exchange X-ray emission resulting from the interaction of stellar wind ions with ISM neutral H provides a direct means of measuring wind mass loss rates [87]. The charge exchange X-ray spectrum is dominated by K-shell emission from H-like and He-like ions of C, O, N, and Ne. These lines are broadened by the wind outflow velocity of 500–1000 km s^{-1} and form broad components underneath the narrower coronal line. A sensitive, low background high-resolution X-ray spectrometer would be able ***to resolve out this charge-exchange signal and simultaneously measure the wind velocity and mass loss rate. This would be new stellar science not feasible at other wavelengths.***

In addition to a relatively steady wind, stars are expected to lose mass in coronal mass ejections (CMEs) accompanying flares. CMEs are also associated with high-energy protons accelerated in the flare and CME shock front. CMEs are very difficult to infer on stars and it is currently unknown how much mass and energy are output in this way on stars other than the Sun, and what CME conditions exoplanets experience.

[88] modeled the effect of a superflare ($E \approx 10^{34}$ erg) and CME impact on a hypothetical Earth-like exoplanet located in the habitable zone (0.16 AU) of the flare star AD Leo (dM3e). High energy protons with energies greater than 10 MeV

severely depleted nitrogen oxides, and subsequently ozone, in the atmosphere for 2 years. [89] found CME energetic particles can create important prebiotic molecules and alter atmospheric greenhouse gases potentially important for the Faint Young Sun paradox.

These studies demonstrate the acute need for observations of stellar CMEs. Extrapolations of solar CME-flare relationships (Fig. 8) are uncertain by orders of magnitude and appear to overestimate large stellar CME candidate kinetic energies. High-resolution spectroscopy at X-ray wavelengths could routinely and definitively *observe the tell-tale Doppler shifts of CMEs or their coronal compression waves* (Fig. 8) *and identify their physical properties, including their thermal structure, masses and energies*, as recently discovered by *Chandra/HETGS* [92]. A combination of high throughput and high spectral resolution is critical for mapping out CME frequency and energy vs optical and X-ray flare diagnostics for exoplanet hosts directly, and generally as a function of spectral type and activity level.

4.2.3 Transmission spectroscopy of exoplanet atmospheres

X-rays are powerful diagnostics of planetary upper atmospheric gas density structure and chemical composition. The transit of the hot Jupiter HD189733b was detected through X-ray absorption by oxygen in *Chandra* observations by [93], who found the scale height of X-ray absorbing gas was higher than suggested by optical and UV transits. Hot Jupiters and similar giant close-in planets are important for improving theory and models describing atmospheric loss.

X-ray absorption measures gas *bulk chemical composition* along the line-of-sight — in this case in the transiting exoplanet atmosphere backlit by the host star's corona. Such measurements are unique to the X-ray range, but only the very closest hot
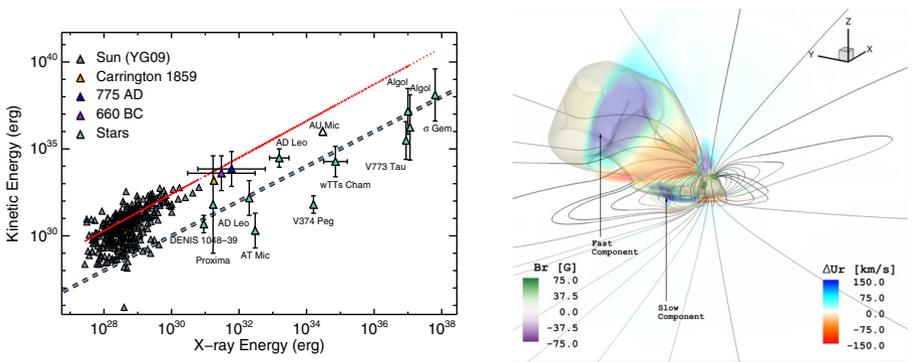

Fig. 8 Left: The kinetic energy vs. associated flare X-ray fluence for solar CMEs and CME candidate events from the literature [90]. Extrapolating the relation to large events on more active stars is extremely uncertain, requiring definitive CME detections and measurements for characterisation. Right: An MHD CME simulation for a moderately active solar-like star [91]. Plasma is compressed and accelerated outward by the CME front, yielding *observable Doppler shifts*, ΔU_r, of up to 100 km s^{-1} or so. Such shifts would be detectable with a sensitive large area grating spectrometer

Jupiters are accessible with *Chandra* and *XMM-Newton*, and then only at low signal-to-noise ratio. A much more sensitive, high spectral resolution observatory will be able to observe HD189733b-like transits out to much greater distances, and by co-adding transits will be able to probe the atmospheres of the nearest terrestrial planets. Absorption edge resonance structure (not resolvable with *Athena*) will distinguish between atomic and molecular or ionised gas, and provide velocity diagnostics for atmospheric outflow. ***X-rays in combination with optical/IR data will provide a powerful probe for clouds and hazes that can confuse IR spectroscopic analyses*** [94].

5 Supernova remnants

Nearby supernova remnants (SNRs), the outcome of SN explosions, are extended sources which allow us to study the structure and chemical composition of the ejecta produced by the explosion. These characteristics reflect somehow the nature of the progenitor star and pristine features of the parent SN that may originate from anisotropies developed at the initiation of the explosion. Observations of SNRs, therefore, encode valuable information about the progenitor star and the SN dynamics.

Studies of SNRs may give exceptional hints on the nature of the shocks between the ejecta and the surrounding medium. Examples of this are the investigation of the broadening of emission lines in ejecta-rich knots, the study of the oxygen rich ejecta-knot of SN 1006 performed by [95] using *XMM-Newton RGS* data, and the more comprehensive study of [96] on the ion-proton temperature ratio using *Chandra* gratings data of SN 1987A.

The studies carried out so far and the already developed state-of-the-art MHD models demonstrate the need for a technological breakthrough to increase the spectral resolution of X-ray instrumentation in order to achieve a better comprehension of a crucial step in the life cycle of elements in the Universe.

To clarify and quantify the required resolution, we have chosen a test case based on real observations of the bright oxygen-rich ejecta knot of the SN 1006, on which an extensive analysis of grating X-ray data has been performed, namely *XMM-Newton RGS* data (Broersen et al., 2013), with the aim to characterise the high resolution spectra and measure the abundances (and therefore the masses) of different elements present in the knot. Bright X-ray knots are ideal laboratories to study how the pristine explosion asymmetries evolve into late-stage SNR morphologies, so the chosen test case is very relevant for the kind of studies *HiReX* will be able to perform.

A 10 ks *HiReX* observation of the knot in SN 1006 would allow us to gain great insight in ***the chemical composition of the knot*** (uncertainties < 0.05 in abundances), ***the electron and ion temperatures of the host rich plasma, and the turbulence and bulk flow of the knot*** with uncertainties on the latter of only $7 \, \mathrm{km \, s^{-1}}$.

6 Compact objects

Outflows are a key ingredient of accretion processes onto compact objects of all masses. In X-ray binaries (XRBs), narrow absorption lines and P-Cygni profiles with velocities of a few hundreds of $km\,s^{-1}$ have been observed almost ubiquitously in high inclination sources, revealing the presence of equatorial winds in these systems. The winds are photoionised and estimates of the expelled mass indicate that it could be large enough to trigger accretion state changes or even be the reason for an outburst to cease [97–99]. A range of ionisations is observed whenever sensitive observations are available, indicating some stratification in the wind (e.g., [100–102]). In particular, a low ionisation component of the wind is present in the majority of XRBs that are not absorbed below ∼2 keV in the interstellar medium [103, see Table 1 in].

Resolving the line profiles provides us with a powerful diagnostic for characterising the winds in XRBs [60, 100]. Line profiles are extensively used at UV, optical, IR or mm wavelengths where resolving powers well above 3000 are available. For example, [104] used them to identify an accelerating wind in pre-main sequence objects as originating from the accretion disc. In addition, the region between 0.2–2 keV contains diagnostic lines for plasma density, like Fe XVII and Fe XXII [105], a crucial parameter to determine the distance between the plasma and the ionising source, which is key to discern among different wind launching mechanisms. Moreover, the wealth of lines in this energy band is also fundamental to diagnose if a plasma is collisionally ionised or photoionised, and thus to differentiate between absorption in the interstellar medium or local to the source.

HiReX will allow a study of the low ionisation wind components at unprecedented resolution in X-rays. For the first time we will be able ***to resolve the line forest between 14–18 Å, determine turbulent and thermal broadening of the lines and measure radial velocities even in the smallest systems***. Only resolving powers of ∼5000 or better, as provided by *HiReX* below 2 keV, will allow us to disentangle line saturation from turbulent and thermal broadening or a blend of the two components of a H-like ion doublet (see Fig. 9). This and the large amount of lines present in the 0.2–2 keV region will allow us to choose non-saturated lines to map the accretion disc atmospheres and winds with exquisite detail. The line spectra from atmospheres (dominated by lines from He-like and H-like elements from C to Fe, radiative recombination lines and Fe L lines) are very sensitive to temperature, ionisation and emission measure of each atmospheric layer, probing the heating mechanisms in the disc [106]. For winds, thermal pressure [107, 108], aided by radiation pressure for systems with luminosities above 50% Eddington, is currently favoured as the main launching mechanism, but the topic of whether there is room for a magnetic wind or not is highly debated (e.g. [109–111]). The high resolution line profiles obtained with *HiReX* (e.g. Fig. 9) will allow us to disentangle between these mechanisms since the wind velocity/acceleration profile is expected to be different for thermal, radiative and magnetic pressure winds [100, 112]. In this sense, ***HiReX will be complementary to Athena by expanding the studies of the highest ionisation component of winds to the lower ionisation ones, but adding fundamental diagnostic parameters such as density.***
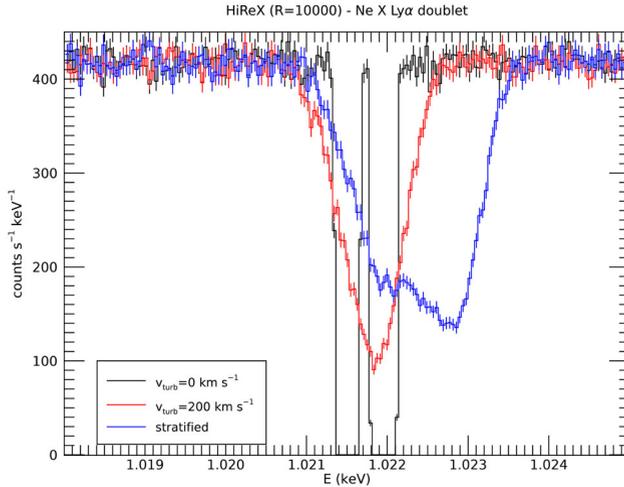
Fig. 9 Ne X line profiles expected for a a thermal wind with no significant turbulence (black), a thermal wind with a turbulence of 200 km s^{-1} (red), and a stratified wind with a velocity profile between 0 and 300 km s^{-1} (blue) and no turbulence. At a resolution lower than $\sim$0.2 eV, the line profiles in black and red will be indistinguishable due to the blend of the line doublet. However, with the resolving power of *HiReX*, we will be able to resolve the velocity profile of the wind (blue) allowing us to make detailed comparisons with the expectations for thermal, radiative or magnetic winds, and to distinguish between a profile with or without turbulence. All diagnostics shown will critically depend on the capability to recognise a saturated line (see text), which otherwise would introduce an unknown systematic uncertainty in the resolution and interpretation of the line profiles

While *Athena* will provide a resolving power close to 3000 at 7 keV, sufficient to resolve line profiles for the most ionised component of the plasma revealed by the presence of Fe XXV and Fe XXVI lines, at energies below 2 keV, only *HiReX* provides the resolving power needed to make the same studies for the lower ionisation components of the wind. Note that the Ne X doublet is only separated by $\sim$0.5 eV, compared to $\sim$20 eV for the Fe XXVI doublet [113]. The recently reported presence of optical winds during the accretion state where jets are observed (e.g., [99, 114]) signals the presence of relatively cool material that could be associated to the soft X-ray wind component. Since the high ionisation wind component is absent in such an accretion state and only appears at states dominated by strong thermal emission, the mechanisms behind the X-ray low and high ionisation components could be different. *HiReX* will allow us ***to fully characterise the low ionisation component of winds and test if the launching mechanism is the same as for the high ionisation winds***. Finally, the line profiles will also allow us to determine the mass loss rate in the wind by constraining the solid angle of the wind through the ratio of emission to absorption.

7 A possible mission concept

Resolving the thermal Doppler width (FWHM) of a transition in an ionic species of atomic mass M in a plasma of temperature T requires a resolving power $R = 9700(M/56)^{1/2}(T/10^6 \text{ K})^{-1/2}$. We choose $R = 10\,000$ as our reference value. At this value, we resolve the lines of Fe ions, the heaviest abundant element, in essentially all X-ray plasmas. Given sufficient photon flux, such resolving power will also enable the measurement of bulk velocities down to a few km s^{-1}.

To maintain an approximately constant resolving power across an extended X-ray energy band, diffractive spectrometers offer the best combination of flexibility and ease of practical implementation. The resolving power of a diffraction grating spectrometer scales approximately inversely proportional to photon energy, that of a microcalorimeter-based spectrometer approximately proportional to photon energy. But a diffraction grating spectrometer can be operated in a series of different spectral orders, essentially as an 'echelle' spectrograph, which allows for a more uniform resolving power coverage of the chosen band. We explore a simple design based on laboratory-proven technology.

Two types of diffraction grating are currently being developed for high-resolution astrophysical X-ray spectroscopy: the Critical Angle Transmission grating [115], and the 'off-plane' radial groove gratings [116]. Very roughly speaking, the first type combines low tolerance alignment implementation with a relatively meticulous manufacturing process, while the second type is faster to manufacture but requires precise optical alignment. Both types offer a natural combination of high dispersion and high diffraction efficiency. We detail a possible design based on CAT gratings.

We choose 100–2000 eV as the baseline energy range. The energy range 500–1000 eV (12–23 Å) is especially rich in astrophysically important transitions (the O K-shell and Fe L shell species), and we blaze the spectrometer at 15 Å. For a grating period $d = 2000$ Å, the angle of incidence on Si grating bars should not exceed 2 degrees, and the spectrometer operates in spectral orders $m \approx 9$ around the blaze wavelength [115]. Order separation can be ensured by reading out the spectroscopic image with a semiconductor imaging detector with an energy resolving power of order 10 or better, such as delivered by a Fano-limited Si device. Assuming a focusing optic with angular resolution ≤ 1 arcsec, and ignoring spherical aberration and the effect of grating imperfections, results in a spectroscopic resolving power at blaze of 14 400. Spectral orders 1–12 provide a resolving power over 10 000 at all wavelengths longer than about 8 Å.

If we assume that systematic effects (uncalibrated pixel-to-pixel quantum efficiency variations) in the focal plane detector are the ultimate limit to the minimum detectable line equivalent width, then, for an assumed 3% systematic error, the minimum detectable equivalent width is 3% of the instrument resolution, or $EW_{\text{limit}} = 3 \times 10^{-2}(\lambda/10\,000) = 3 \times 10^{-6}\lambda$ Å$= 0.06(\lambda/20\text{Å})$ mÅ.

Table 1 compares the figure of merit (expected significance) of weak line detections for various instruments. In this respect *HiReX* is 20–50 times better than the present grating spectrometers. While *Athena*/*X-IFU* can compensate the lower spectral resolution by more effective area in terms of statistical significance of line detections, the ultimate limit for weak lines is determined by the systematic uncertainties outlined above. Assuming a typical 3% systematic uncertainty for all these

Table 1 Figure of Merit (FoM) for measuring equivalent widths of weak lines at 0.5 keV energy for various high-resolution X-ray spectrometers

Mission	Instrument	A_{eff} (cm2)	R	FoM
HiReX		1 500	10 000	$\equiv 1$
Chandra	*LETGS*	12	500	0.02
XMM-Newton	*RGS*	90	400	0.05
XRISM	*Resolve*	125	100	0.03
Athena	*X-IFU*	5 900	200	0.28

The expected detection significance scales with FoM $\sim \sqrt{A_{\mathrm{eff}} R}$ with A_{eff} the effective area and R the resolution of the instrument

instruments, the ultimate performance is then determined solely by the resolving power R. ***In this respect, for detection of weak lines, HiReX is better than all other instruments by a factor of 20–50.***

8 Conclusions

The scope of this paper, part of the ESA "Voyage-2050" call for White Papers, is to highlight the importance of High Resolution Spectroscopy in the soft X-ray band to investigate and solve most of the still open astrophysical problems that will be central in the next decades and for which a deep understanding of ***the Universe's wandering metals, their physical and kinematical states, and their chemical composition*** represents the only viable solution.

We presented a medium-size mission-concept (*HiReX*) consisting in a very high spectral resolution (R≥ 10, 000) soft X-ray (0.1−2 keV dispersive spectrometer, able to resolve the thermal widths of medium-to-high-ionization astrophysically abundant metal ions. With its relatively large effective area (1500 cm2 at 1 keV) and extreme (for X-ray standards) resolving power (R≥ 10, 000), *HiReX* improves the detectability of weak emission and absorption lines by a factor of 20–50, compared to any other existing or already planned instrument.

References

1. Rauch, M.: ARA&A **36**, 267–316 (1998)
2. Weinberg, D.H., Miralda-Escudé, J., Hernquist, L., Katz, N.: ApJ **490**(2), 564 (1997)
3. Cen, R., Ostriker, J.P.: ApJ **650**(2), 560 (2006)
4. Schaye, J., Crain, R.A., Bower, R.G., Furlong, M., Schaller, M., Theuns, T., Dalla Vecchia, C., Frenk, C.S., McCarthy, I.G., Helly, J.C., Jenkins, A., Rosas-Guevara, Y.M., White, S.D.M., Baes, M., Booth, C.M., Camps, P., Navarro, J.F., Qu, Y., Rahmati, A., Sawala, T., Thomas, P.A., Trayford, J.: MNRAS **446**(1), 521–554 (2015)
5. Cen, R., Fang, T.: ApJ **650**(2), 573–591 (2006)
6. Fang, T., Bryan, G.L., Canizares, C.R.: ApJ **564**(2), 604–623 (2002)
7. Wijers, N.A., Schaye, J., Oppenheimer, B.D., Crain, R.A., Nicastro, F.: MNRAS, 1704 (2019)
8. Nicastro, F., Krongold, Y., Mathur, S., Elvis, M.: Astron. Nachrichten **338**(281), 281–286 (2017)
9. Bonamente, M., Nevalainen, J., Tilton, E., Liivamägi, J., Tempel, E., Heinämäki, P., Fang, T.: MNRAS **457**(4), 4236–4247 (2016)
10. Nicastro, F., Kaastra, J., Krongold, Y., Borgani, S., Branchini, E., Cen, R., Dadina, M., Danforth, C.W., Elvis, M., Fiore, F., Gupta, A., Mathur, S., Mayya, D., Paerels, F., Piro, L., Rosa-Gonzalez, D., Schaye, J., Shull, J.M., Torres-Zafra, J., Wijers, N., Zappacosta, L.: Nature **558**(7710), 406–409 (2018)
11. Freeman, P., Doe, S., Siemiginowska, A.: In: Starck, J.-L., Murtagh, F.D. (eds.) Society of Photo-Optical Instrumentation Engineers (SPIE) Conference Series, vol. 4477, pp. 76–87. Proc. SPIE (2001)
12. Crain, R.A., Schaye, J., Bower, R.G., Furlong, M., Schaller, M., Theuns, T., Dalla Vecchia, C., Frenk, C.S., McCarthy, I.G., Helly, J.C., Jenkins, A., Rosas-Guevara, Y.M., White, S.D.M., Trayford, J.W.: MNRAS **450**(2), 1937–1961 (2015)
13. Churazov, E., Haehnelt, M., Kotov, O., Sunyaev, R.: MNRAS **323**(1), 93–100 (2001)
14. Khabibullin, I., Churazov, E.: MNRAS **482**(4), 4972–4984 (2019)
15. Barcons, X., Barret, D., Decourchelle, A., den Herder, J.W., Fabian, A.C., Matsumoto, H., Lumb, D., Nandra, K., Piro, L., Smith, R.K., Willingale, R.: Astron. Nachrichten **338**, 153–158 (2017)
16. Maller, A.H., Bullock, J.S.: MNRAS **355**(3), 694–712 (2004)
17. McGaugh, S.S., Schombert, J.M., de Blok, W.J.G., Zagursky, M.J.: ApJ **708**, L14–L17 (2010)
18. Fang, T., Bullock, J., Boylan-Kolchin, M.: ApJ **762**(1), 20 (2013)
19. Miller, M.J., Bregman, J.N.: ApJ **800**(1), 14 (2015)
20. Faerman, Y., Sternberg, A., McKee, C.F.: ApJ **835**(1), 52 (2017)
21. Bregman, J.N., Anderson, M.E., Miller, M.J., Hodges-Kluck, E., Dai, X., Li, J.-T., Li, Y., Qu, Z.: ApJ **862**(1), 3 (2018)
22. Hodges-Kluck, E.J., Miller, M.J., Bregman, J.N.: ApJ **822**, 21 (2016)
23. Miller, M.J., Hodges-Kluck, E.J., Bregman, J.N.: ApJ **818**, 112 (2016)
24. Schechter, P.: ApJ **203**, 297–306 (1976)
25. Bregman, J.N., Alves, G.C., Miller, M.J., Hodges-Kluck, E.: J. Astron. Telesc. Instrum. Syst. **1**(4), 045003 (2015)
26. Ma, Y.-Z., Van Waerbeke, L., Hinshaw, G., Hojjati, A., Scott, D., Zuntz, J.: J. Cosmol. Astropart. Phys. **2015**(9), 046 (2015)
27. Peeples, M.S., Werk, J.K., Tumlinson, J., Oppenheimer, B.D., Prochaska, J.X., Katz, N., Weinberg, D.H.: ApJ **786**, 54 (2014)

28. Savage, B.D., Sembach, K.R., Wakker, B.P., Richter, P., Meade, M., Jenkins, E.B., Shull, J.M., Moos, H.W., Sonneborn, G.: ApJS **146**(1), 125–164 (2003)
29. Werk, J.K., Prochaska, J.X., Cantalupo, S., Fox, A.J., Oppenheimer, B., Tumlinson, J., Tripp, T.M., Lehner, N., McQuinn, M.: ApJ **833**(1), 54 (2016)
30. Sokołowska, A., Babul, A., Mayer, L., Shen, S., Madau, P.: ApJ **867**(1), 73 (2018)
31. Lagos, C.P., Theuns, T., Stevens, A.R.H., Cortese, L., Padilla, N.D., Davis, T.A., Contreras, S., Croton, D.: MNRAS **464**(4), 3850–3870 (2017)
32. Urban, O., Werner, N., Allen, S.W., Simionescu, A., Mantz, A.: MNRAS **470**(4), 4583–4599 (2017)
33. Biffi, V., Planelles, S., Borgani, S., Rasia, E., Murante, G., Fabjan, D., Gaspari, M.: MNRAS **476**(2), 2689–2703 (2018)
34. Biffi, V., Mernier, F., Medvedev, P.: Space Sci.Rev. **214**(8), 123 (2018)
35. Mernier, F., Biffi, V., Yamaguchi, H., Medvedev, P., Simionescu, A., Ettori, S., Werner, N., Kaastra, J.S., de Plaa, J., Gu, L.: SpaceSci.Rev. **214**(8), 129 (2018)
36. Fabjan, D., Borgani, S., Tornatore, L., Saro, A., Murante, G., Dolag, K.: MNRAS **401**(3), 1670 (2010)
37. McCarthy, I.G., Schaye, J., Bower, R.G., Ponman, T.J., Booth, C.M., Dalla Vecchia, C., Springel, V.: MNRAS **412**(3), 1965–1984 (2011)
38. Cucchetti, E., Pointecouteau, E., Peille, P., Clerc, N., Rasia, E., Biffi, V., Borgani, S., Tornatore, L., Dolag, K., Roncarelli, M., Gaspari, M., Ettori, S., Bulbul, E., Dauser, T., Wilms, J., Pajot, F., Barret, D.: A&A **620**, A173 (2018)
39. Simionescu, A., ZuHone, J., Zhuravleva, I., Churazov, E., Gaspari, M., Nagai, D., Werner, N., Roediger, E., Canning, R., Eckert, D., Gu, L., Paerels, F.: Space Sci.Rev. **215**(2), 24 (2019)
40. Kaastra, J.S., Mewe, R., Liedahl, D.A., Komossa, S., Brinkman, A.C.: A&A **354**, L83–L86 (2000)
41. Kaspi, S., Brandt, W.N., George, I.M., Netzer, H., Crenshaw, D.M., Gabel, J.R., Hamann, F.W., Kaiser, M.E., Koratkar, A., Kraemer, S.B.: ApJ **574**(2), 643–662 (2002)
42. Blustin, A.J., Page, M.J., Fuerst, S.V., Brand uardi-Raymont, G., Ashton, C.E.: A&A **431**, 111–125 (2005)
43. Liedahl, D.A.: The X-Ray Spectral Properties of Photoionized Plasma and Transient Plasmas. In: van Paradijs, J., Bleeker, J.A.M. (eds.) X-Ray Spectroscopy in Astrophysics, Lectures held at the Astrophysics School X. Organized by the European Astrophysics Doctoral Network (EADN) in Amsterdam, the Netherlands. September 22 - October 3, 1997. Edited by Jan van Paradijs and Johan A. M. Bleeker. Lecture Notes in Physics, Vol. 520, Springer, 1999., p.189, vol. 520, p. 189 (1999)
44. Porquet, D., Dubau, J., Grosso, N.: SpaceSci.Rev. **157**(1-4), 103–134 (2010)
45. Tombesi, F., Cappi, M., Reeves, J.N., Palumbo, G.G.C., Yaqoob, T., Braito, V., Dadina, M.: A&A **521**, A57 (2010)
46. Gofford, J., Reeves, J.N., Tombesi, F., Braito, V., Turner, T.J., Miller, L., Cappi, M.: MNRAS **430**(1), 60–80 (2013)
47. Proga, D., Stone, J.M., Kallman, T.R.: ApJ **543**(2), 686–696 (2000)
48. Kato, Y., Mineshige, S., Shibata, K.: ApJ **605**(1), 307–320 (2004)
49. Fukumura, K., Tombesi, F., Kazanas, D., Shrader, C., Behar, E., Contopoulos, I.: ApJ **805**(1), 17 (2015)
50. Tombesi, F., Meléndez, M., Veilleux, S., Reeves, J.N., González-Alfonso, E., Reynolds, C.S.: Nature **519**(7544), 436–438 (2015)
51. Feruglio, C., Fiore, F., Carniani, S., Piconcelli, E., Zappacosta, L., Bongiorno, A., Cicone, C., Maiolino, R., Marconi, A., Menci, N.: A&A **583**, A99 (2015)
52. Longinotti, A.L., Krongold, Y., Guainazzi, M., Giroletti, M., Panessa, F., Costantini, E., Santos-Lleo, M., Rodriguez-Pascual, P.: ApJ **813**(2), L39 (2015)
53. Reeves, J.N., Lobban, A., Pounds, K.A.: ApJ **854**(1), 28 (2018)
54. Danehkar, A., Nowak, M.A., Lee, J.C., Kriss, G.A., Young, A.J., Hardcastle, M.J., Chakravorty, S., Fang, T., Neilsen, J., Rahoui, F.: ApJ **853**(2), 165 (2018)
55. Pinto, C., Alston, W., Parker, M.L., Fabian, A.C., Gallo, L.C., Buisson, D.J.K., Walton, D.J., Kara, E., Jiang, J., Lohfink, A.: MNRAS **476**(1), 1021–1035 (2018)
56. Serafinelli, R., Tombesi, F., Vagnetti, F., Piconcelli, E., Gaspari, M., Saturni, F.G.: arXiv:1906.02765 (2019)
57. Mehdipour, M., Kaastra, J.S., Kriss, G.A., Arav, N., Behar, E., Bianchi, S., Branduardi-Raymont, G., Cappi, M., Costantini, E., Ebrero, J.: A&A **607**, A28 (2017)
58. Fiore, F., Feruglio, C., Shankar, F., Bischetti, M., Bongiorno, A., Brusa, M., Carniani, S., Cicone, C., Duras, F., Lamastra, A.: A&A **601**, A143 (2017)

59. Nicastro, F., Fiore, F., Perola, G.C., Elvis, M.: ApJ **512**(1), 184–196 (1999)
60. Kaastra, J.S., Kriss, G.A., Cappi, M., Mehdipour, M., Petrucci, P.O., Steenbrugge, K.C., Arav, N., Behar, E., Bianchi, S., Boissay, R., Brand uardi-Raymont, G., Chamberlain, C., Costantini, E., Ely, J.C., Ebrero, J., Di Gesu, L., Harrison, F.A., Kaspi, S., Malzac, J., De Marco, B., Matt, G., Nand ra, K., Paltani, S., Person, R., Peterson, B.M., Pinto, C., Ponti, G., Nuñez, F.P., De Rosa, A., Seta, H., Ursini, F., de Vries, C.P., Walton, D.J., Whewell, M.: Science **345**(6192), 64 (2014)
61. Min, M., Waters, L.B.F.M., de Koter, A., Hovenier, J.W., Keller, L.P., Markwick-Kemper, F.: A&A **462**(2), 667 (2007)
62. Juett, A.M., Schulz, N.S., Chakrabarty, D.: ApJ **612**, 308 (2004)
63. Juett, A.M., Schulz, N.S., Chakrabarty, D., Gorczyca, T.W.: ApJ **648** (September 2006)
64. Yao, Y., Schulz, N.S., Gu, M.F., Nowak, M.A., Canizares, C.R.: ApJ **696**, 1418 (2009)
65. Lee, J.C., Ravel, B.: ApJ **622**(2), 970 (2005)
66. Lee, J.C., Xiang, J., Ravel, B., Kortright, J., Flanagan, K.: ApJ **702**, 970 (2009)
67. de Vries, C.P., Costantini, E.: A&A **497**, 393 (2009)
68. Pinto, C., Kaastra, J.S., Costantini, E., Verbunt, F.: A&A **521**, A79 (2010)
69. Pinto, C., Kaastra, J.S., Costantini, E., de Vries, C.: A&A **551**, A25 (2013)
70. Zeegers, S.T., Costantini, E., de Vries, C.P., Tielens, A.G.G.M., Chihara, H., de Groot, F., Mutschke, H., Waters, L.B.F.M., Zeidler, S.: A&A **599**, A117 (2017)
71. Rogantini, D., Costantini, E., Zeegers, S.T., de Vries, C.P., Bras, W., de Groot, F., Mutschke, H., Watersx, L.B.F.M.: A&A **609**, A22 (2018)
72. García, J., Mendoza, C., Bautista, M.A., Gorczyca, T.W., Kallman, T.R., Palmeri, P.: ApJS **158**(1), 68 (2005)
73. Gatuzz, E., García, J., Mendoza, C., Kallman, T.R., Witthoeft, M., Lohfink, A., Bautista, M.A., Palmeri, P., Quinet, P.: ApJ **768**(1), 60 (2013)
74. Heilmann, R.K., Bruccoleri, A.R., Song, J., Kolodziejczak, J., Gaskin, J.A., O'Dell, S.L., Cheimetz, P., Hertz, E., Smith, R.K., Burwitz, V., Hartner, G., La Caria, M.-M., Schattenburg, M.L.: In: Proc. SPIE, vol. 10399, p. 1039914. Society of Photo-Optical Instrumentation Engineers (SPIE) Conference Series (2017)
75. Güdel, M., Nazé, Y.: A&A Rev. **17**(3), 309–408 (2009)
76. Hervé, A., Rauw, G., Nazé, Y.: A&A **551**, A83 (2013)
77. Barret, D., Cappi, M.: A&A, in press. arXiv:1906.02734 (2019)
78. Argiroffi, C., Drake, J.J., Bonito, R., Orlando, S., Peres, G., Miceli, M.: A&A **607**, A14 (2017)
79. Donati, J.F., Gregory, S.G., Alencar, S.H.P., Bouvier, J., Hussain, G., Skelly, M., Dougados, C., Jardine, M.M., Ménard, F., Romanova, M.M.: MNRAS **417**(1), 472–487 (2011)
80. Owen, J.E., Jackson, A.P.: MNRAS **425**, 2931–2947 (2012)
81. Garraffo, C., Drake, J.J., Cohen, O.: ApJ **833**, L4 (2016)
82. Dong, C., Lingam, M., Ma, Y., Cohen, O.: ApJ **837**, L26 (2017)
83. Garcia-Sage, K., Glocer, A., Drake, J.J., Gronoff, G., Cohen, O.: ApJ **844**, L13 (2017)
84. Airapetian, V.S., Glocer, A., Khazanov, G.V., Loyd, R.O.P., France, K., Sojka, J., Danchi, W.C., Liemohn, M.W.: ApJ **836**, L3 (2017)
85. Brain, D.A., Bagenal, F., Ma, Y.-J., Nilsson, H., Stenberg Wieser, G.: J. Geophys. Res. (Planets) **121**, 2364–2385 (2016)
86. Wood, B.E., Müller, H.-R., Redfield, S., Edelman, E.: ApJ **781**, L33 (2014)
87. Wargelin, B.J., Drake, J.J.: ApJ **578**, 503 (2002)
88. Segura, A., Walkowicz, L.M., Meadows, V., Kasting, J., Hawley, S.: Astrobiology **10**, 751 (2010)
89. Airapetian, V.S., Glocer, A., Gronoff, G., Hébrard, E., Danchi, W.: Nat. Geosci. **9**, 452 (2016)
90. Moschou, S.-P., Drake, J.J., Cohen, O., Alvarado-Gómez, J.D., Garraffo, C., Fraschetti, F.: ApJ **877**(2), 105 (2019)
91. Alvarado-Gómez, J.D., Drake, J.J., Cohen, O., Moschou, S.P., Garraffo, C.: ApJ **862**, 93 (2018)
92. Argiroffi, C., Reale, F., Drake, J.J., Ciaravella, A., Testa, P., Bonito, R., Miceli, M., Orlando, S., Peres, G.: Nat. Astron., 328 (2019)
93. Poppenhaeger, K., Schmitt, J.H.M.M., Wolk, S.J.: ApJ **773**, 62 (2013)
94. Sing, D.K., Fortney, J.J., Nikolov, N., Wakeford, H.R., Kataria, T., Evans, T.M., Aigrain, S., Ballester, G.E., Burrows, A.S., Deming, D., Désert, J.-M., Gibson, N.P., Henry, G.W., Huitson, C.M., Knutson, H.A., Lecavelier Des Etangs, A., Pont, F., Showman, A.P., Vidal-Madjar, A., Williamson, M.H., Wilson, P.A.: Nature **529**, 59–62 (January 2016)
95. Broersen, S., Vink, J., Miceli, M., Bocchino, F., Maurin, G., Decourchelle, A.: A&A **552**, A9 (2013)

96. Miceli, M., Orlando, S., Burrows, D.N., Frank, K.A., Argiroffi, C., Reale, F., Peres, G., Petruk, O., Bocchino, F.: Nat. Astron. **3**, 236–241 (2019)
97. Shields, G.A., McKee, C.F., Lin, D.N.C., Begelman, M.C.: ApJ **306**, 90 (1986)
98. Ponti, G., Fender, R.P., Begelman, M.C., Dunn, R.J.H., Neilsen, J., Coriat, M.: MNRAS **422**(1), L11–L15 (2012)
99. Muñoz-Darias, T., Casares, J., Mata Sánchez, D., Fender, R.P., Armas Padilla, M., Linares, M., Ponti, G., Charles, P.A., Mooley, K.P., Rodriguez, J.: Nature **534**(7605), 75–78 (2016)
100. Ueda, Y., Murakami, H., Yamaoka, K., Dotani, T., Ebisawa, K.: ApJ **609**(1), 325–334 (2004)
101. Miller, J.M., Raymond, J., Homan, J., Fabian, A.C., Steeghs, D., Wijnands, R., Rupen, M., Charles, P., van der Klis, M., Lewin, W.H.G.: ApJ **646**(1), 394–406 (2006)
102. Kallman, T.R., Bautista, M.A., Goriely, S., Mendoza, C., Miller, J.M., Palmeri, P., Quinet, P., Raymond, J.: ApJ **701**(2), 865–884 (2009)
103. Díaz Trigo, M., Boirin, L.: Astron. Nachrichten **337**(4-5), 368 (2016)
104. Calvet, N., Hartmann, L., Kenyon, S.J.: ApJ **402**, 623 (1993)
105. Mauche, C.W., Liedahl, D.A., Fournier, K.B.: In: Vrielmann, S., Cropper, M. (eds.) IAU Colloq. 190: Magnetic Cataclysmic Variables, vol. 315, p. 124. Astronomical Society of the Pacific Conference Series (2004)
106. Jimenez-Garate, M.A., Raymond, J.C., Liedahl, D.A.: ApJ **581**(2), 1297–1327 (2002)
107. Begelman, M.C., McKee, C.F., Shields, G.A.: ApJ **271**, 70–88 (1983)
108. Begelman, M.C., McKee, C.F.: ApJ **271**, 89–112 (1983)
109. Done, C., Tomaru, R., Takahashi, T.: MNRAS **473**(1), 838 (2018)
110. Fukumura, K., Kazanas, D., Shrader, C., Behar, E., Tombesi, F., Contopoulos, I.: ApJ **864**(2), L27 (2018)
111. Waters, T., Proga, D.: MNRAS **481**(2), 2628 (2018)
112. Fukumura, K., Kazanas, D., Contopoulos, I., Behar, E.: ApJ **715**(1), 636 (2010)
113. Verner, D.A., Verner, E.M., Ferland, G.J.: At. Data Nucl. Data Tables **64**, 1 (1996)
114. Rahoui, F., Coriat, M., Lee, J.C.: MNRAS **442**(2), 1610 (2014)
115. Heilmann, R.K., Kolodziejczak, J., Bruccoleri, A.R., Gaskin, J.A., Schattenburg, M.L.: Appl. Opt. **58**(5), 1223 (2019)
116. McEntaffer, R.L.: J. Astron. Telesc. Instrum. Syst. **5**, 021002 (2019)

Affiliations

F. Nicastro[1] · J. Kaastra[2] · C. Argiroffi[3] · E. Behar[4] · S. Bianchi[5] · F. Bocchino[6] ·
S. Borgani[7] · G. Branduardi-Raymont[8] · J. Bregman[9] · E. Churazov[10,11] ·
M. Diaz-Trigo[12] · C. Done[13] · J. Drake[14] · T. Fang[15] · N. Grosso[16] ·
A. Luminari[17,1] · M. Mehdipour[2] · F. Paerels[18] · E. Piconcelli[1] · C. Pinto[19] ·
D. Porquet[16] · J. Reeves[20] · J. Schaye[21] · S. Sciortino[6] · R. Smith[14] · D. Spiga[22] ·
R. Tomaru[23] · F. Tombesi[17] · N. Wijers[21] · L. Zappacosta[1]

[1] Istituto Nazionale di Astrofisica - Osservatorio Astronomico di Roma (INAF - OAR),
     Via di Frascati 33, 00078 Monte Porzio Catone (RM), Italy
[2] Netherlands Institute for Space Reasearch (SRON), Sorbonnelaan 2, 3584 CA Utrecht,
     The Netherlands
[3] University of Palermo, Palermo, Italy
[4] Technion, Hiafa, Israel
[5] Universitá degli Studi RomaTre, Roma, Italy
[6] INAF - OAPA, Palermo, Italy
[7] Mullard Space Science Laboratory, Holmbury St. Mary, UK
[8] MSSL, Noida, UK
[9] University of Michigan, Ann Arbor, MI, USA
[10] MPA, Garching, Germany
[11] IKI, Moscow, Russia
[12] ESO, Müchen, Germany
[13] University of Durham, Durham, UK
[14] SAO - CfA, Cambridge, MA, USA
[15] Xiamen University, Xiamen, China
[16] Aix Marseille University, CNRS, CNES, LAM, Marseille, France
[17] University of Rome "Tor-Vergata", Rome, Italy
[18] Columbia University, New York, NY, USA
[19] INAF-IASF, Palermo, Italy
[20] University of Maryland, College Park, MD, USA
[21] Leiden Observatory, Leiden, The Netherlands
[22] INAF-OA-Brera, Milan, Italy
[23] University of Tokyo, Tokyo, Japan